Fluorescence-Based Detection of Raloxifene Using Green-Synthesized Carbon Quantum Dots from Acer monspessulanum: Optimization via Experimental Design and Machine Learning

Neda Alaei
Department of Biology, Sa.C.,
Bahareh Rahimian Zarif
bahareh_r_z@yahoo.com

Department of Biology, Sa.C.,
Nahid Haghnazari
Department of Biology, Sa.C.,

Research Article

Keywords: Carbon quantum dots, Acer monspessulanum, Raloxifene detection, Fluorescence sensor, Experimental design, Machine learning, Antibiotic monitoring

Posted Date: March 26th, 2026

DOI: https://doi.org/10.21203/rs.3.rs-8820235/v1

Additional Declarations: No competing interests reported.

Abstract

In this study, carbon quantum dots (CQDs) were synthesized through a green hydrothermal method using *Acer monspessulanum* leaf extract as a natural, renewable carbon source. The synthesized CQDs were thoroughly characterized using fluorescence spectroscopy, FTIR, SEM, EDX, and elemental mapping techniques to confirm their structural and optical features. The resulting nanomaterial exhibited strong and stable fluorescence emission, which was effectively quenched in the presence of raloxifene (RLX), enabling its sensitive detection based on a fluorescence quenching mechanism. Experimental parameters influencing sensor performance were systematically optimized using Design-Expert software in combination with Response Surface Methodology (RSM), yielding a linear detection range of 10.0 to 750.0 μM, with a low limit of detection (LOD) of 1.27 μM and a limit of quantification (LOQ) of 3.82 μM. The developed fluorescence sensor demonstrated excellent repeatability (RSD = 0.092%, n = 10) and reproducibility (RSD = 0.092%), indicating its robustness for routine analysis. Furthermore, machine learning algorithms were employed to enhance model prediction accuracy and to support deeper insight into the complex interactions between experimental variables. The applicability of the sensing platform was successfully validated through the detection of raloxifene in spiked real samples, with negligible matrix effects and satisfactory recovery values. These findings highlight the potential of the CQDs-based sensor as an eco-friendly, cost-effective, and high-performance tool for monitoring pharmaceutical residues in biological and environmental matrices.

Introduction

Raloxifene is a selective estrogen receptor modulator (SERM) widely prescribed for the prevention and treatment of osteoporosis in postmenopausal women, as well as for reducing the risk of invasive breast cancer in high-risk populations. Despite its therapeutic benefits, raloxifene exhibits poor water solubility and variable bioavailability, which can lead to inconsistent pharmacokinetics and potential accumulation in biological systems. Moreover, its widespread use and excretion in unmetabolized or partially metabolized forms have raised concerns regarding its presence in environmental water bodies and pharmaceutical wastewater. From an analytical perspective, the detection and quantification of raloxifene are critical for several reasons. First, precise monitoring of raloxifene levels in pharmaceutical formulations is essential to ensure dosage accuracy and therapeutic efficacy. Second, surveillance of raloxifene residues in biological samples—such as serum, urine, or breast milk—is important for pharmacokinetic studies and patient compliance monitoring. Third, the identification of raloxifene in environmental matrices, including wastewater and surface water, has become increasingly relevant due to the emergence of pharmaceuticals as micropollutants with endocrine-disrupting potential.

Traditional analytical techniques such as high-performance liquid chromatography (HPLC) [1, 2], spectrophotometry[3], reverse phase HPLC [4], chemiluminescence, and electrochemical [5, 6] have been employed for raloxifene detection. However, these methods often require complex sample preparation, expensive instrumentation, and time-consuming procedures. As a result, there is a growing demand for alternative sensing platforms that offer high sensitivity, rapid response, cost-effectiveness, and

environmental compatibility. Fluorescence-based nanosensors, particularly those utilizing carbon quantum dots (CQDs), have emerged as promising tools for the trace-level detection of pharmaceutical compounds due to their tunable photoluminescence, low toxicity, and facile surface functionalization. The development of green, sustainable, and selective sensing approaches for raloxifene detection is not only beneficial for pharmaceutical quality control but also contributes to environmental monitoring and public health protection. Therefore, designing eco-friendly CQD-based sensors with optimized performance through advanced chemometric tools represents a timely and impactful research direction [7, 8].

In recent years, green synthesis strategies have gained significant attention as environmentally friendly alternatives to conventional nanomaterial fabrication methods, which often rely on toxic reagents, high energy inputs, and hazardous byproducts [9]. Green synthesis leverages natural, renewable, and biodegradable resources—such as plant extracts, fruit peels, and microbial metabolites—as reducing, stabilizing, and carbonizing agents, aligning with the principles of green chemistry. These approaches not only minimize environmental impact but also impart beneficial surface functionalities to the resulting nanomaterials, enhancing their biocompatibility and sensing performance. Among various natural precursors, plant-based sources are particularly attractive due to their abundance of phytochemicals, including polyphenols, flavonoids, and organic acids, which facilitate efficient carbonization and surface passivation. *Acer monspessulanum*, a Mediterranean tree species rich in bioactive compounds, presents a promising and underexplored candidate for the green synthesis of carbon quantum dots (CQDs). Utilizing such botanical precursors supports sustainable nanotechnology development while enabling tailored optical and chemical properties for advanced analytical applications [10, 11].

Fluorescence-based sensing techniques have emerged as powerful tools in analytical chemistry due to their high sensitivity, rapid response, and non-destructive nature. Unlike conventional detection methods, such as electrochemical or chromatographic techniques, fluorescence sensors enable real-time monitoring of analytes at trace levels without the need for extensive sample preparation. Carbon quantum dots (CQDs), as novel fluorescent nanomaterials, offer additional advantages, including excellent photostability, low cytotoxicity, tunable emission wavelengths, and facile surface functionalization. These features make CQDs particularly suitable for the development of selective and sensitive sensors for pharmaceutical compounds. Moreover, the fluorescence quenching or enhancement behavior of CQDs in response to target analytes provides a straightforward and cost-effective signal transduction mechanism. When combined with green synthesis approaches, CQD-based fluorescence sensors represent a sustainable and efficient platform for applications in pharmaceutical analysis, environmental monitoring, and biomedical diagnostics. [12]. The performance of fluorescence-based sensors is highly influenced by multiple experimental parameters, including pH, reaction time, temperature, precursor concentration, and analyte interaction conditions. To achieve optimal sensor performance, systematic optimization strategies such as Design of Experiments (DoE) and Response Surface Methodology (RSM) are employed to model complex variable interactions, reduce experimental trials, and maximize analytical response. These chemometric tools not only enhance the reliability and reproducibility of the sensor but also contribute to its scalability and practical implementation. In recent

years, machine learning (ML) techniques have been increasingly integrated into analytical chemistry to improve data interpretation, pattern recognition, and predictive modeling. Algorithms such as artificial neural networks (ANN), support vector machines (SVM), and decision trees can extract non-linear relationships from high-dimensional data, providing deeper insights beyond traditional statistical methods. The combination of experimental design with ML-driven analysis thus offers a robust framework for developing high-performance, intelligent sensing systems tailored to specific analytical challenges.

The present study aims to develop an eco-friendly and sensitive fluorescence sensor for the detection of raloxifene using carbon quantum dots synthesized via a green hydrothermal method from Acer monspessulanum leaf extract. The research focuses on comprehensive characterization of the CQDs' structural and optical properties, followed by the optimization of sensing parameters through Design-Expert software coupled with Response Surface Methodology (RSM). Furthermore, advanced machine learning algorithms are integrated to enhance predictive accuracy and interpret complex sensor data. Finally, the practical applicability of the developed sensor is validated by detecting raloxifene in real samples, demonstrating its potential as a cost-effective, sustainable, and high-performance analytical tool for pharmaceutical monitoring and environmental safety.

Experimental

2.1. Reagents and materials

Acer monspessulanum leaves were collected during the autumn season, thoroughly washed, shade-dried, and ground into a fine powder. To prepare the aqueous plant extract, a measured amount of the dried material was boiled in distilled water under controlled conditions. All chemicals and reagents used in this study, including phenobarbital, isoniazid, nevirapine, efavirenz, tenofovir, phenol, thiourea, glucose, catechol, L-cysteine, raloxifene, sumatriptan, Calcium (Ca^{2+}), Potassium (K^{+}), Sodium (Na^{+}), Glucose, Albumin, Ascorbic acid (Vitamin C), Riboflavin (Vitamin B2), Triglycerides, and Lactic acid—were included for interference and sensing studies and were sourced from the same supplier. The pH of all prepared solutions was carefully adjusted to 6.0 using 0.1 M solutions of phosphoric acid, sodium phosphate, hydrochloric acid, or sodium hydroxide, as required. All working solutions were freshly prepared using double-distilled water to maintain analytical accuracy and reproducibility.

2.2 Synthesis of Carbon Quantum Dots (CQDs)

Carbon quantum dots (CQDs) were synthesized via a green hydrothermal method using an aqueous extract of *Acer monspessulanum* leaves as the natural carbon source. Initially, dried leaf powder was mixed with deionized water and heated under reflux to obtain the plant extract. A specific volume of this extract was transferred into a Teflon-lined stainless steel autoclave and subjected to hydrothermal treatment at 180 °C for 6 hours. After cooling to room temperature, the dark brown solution was centrifuged at 10,000 rpm for 15 minutes to remove large particulates. The resulting supernatant was

filtered through a 0.22 µm membrane to isolate uniformly dispersed CQDs. Finally, the fluorescent CQD solution was stored at 4 °C for further characterization and sensing experiments.

2.3 Characterization Techniques

A comprehensive suite of analytical techniques was employed to investigate the structural, morphological, and optical features of the synthesized carbon quantum dots. Fluorescence properties were evaluated using a PerkinElmer LS 45 spectrofluorometer, while UV-Vis absorption measurements were performed with a Cary 100 spectrophotometer to assess optical behavior. Functional group analysis was carried out using Fourier-transform infrared (FTIR) spectroscopy with a Thermo Avatar system, enabling identification of surface chemical bonds. The morphology, particle distribution, and surface texture of the CQDs were visualized through field emission scanning electron microscopy (FE-SEM, TESCAN MIRA III, operating at 15 kV). Elemental composition and spatial distribution of elements were further analyzed using energy-dispersive X-ray spectroscopy (EDX), supported by elemental mapping and line scan profiling to ensure compositional uniformity.

2.4 Experimental Design and Optimization

To systematically optimize the operational parameters influencing the fluorescence sensing efficiency of the CQDs-based sensor, a Central Composite Design (CCD) was applied using Design-Expert software (v11.1.1.0, USA). Three critical factors—solution pH (ranging from 3.0 to 9.0), incubation time (3.0 to 15 minutes), and sensing temperature (30–60 °C)—were selected as independent variables. A total of 20 experimental runs were conducted, incorporating factorial points, axial points, and six center replicates to ensure model robustness, as detailed in Table 1. The experimental data were fitted to a second-order polynomial regression model (**Equation 1**), which accounted for linear, quadratic, and interaction terms between variables.

$$Y=\beta_0+\beta_1A+\beta_2B+\beta_3C+\beta_{11}A_2+\beta_{22}B_2+\beta_{33}C_2+\beta_{12}AB+\beta_{13}AC+\beta_{23}BC \qquad \textbf{Eq. 1}$$

In this model, Y represents the predicted fluorescence intensity, while A (pH), B (temperature), and C (reaction time) are the coded variables. The coefficients (β) reflect the magnitude and direction of individual and combined effects. Model adequacy and statistical significance were assessed via ANOVA at a 95% confidence level ($p < 0.05$). Additionally, three-dimensional surface plots were generated to visualize variable interactions and determine the optimal sensing conditions.

Table 1

2.5 Fluorescence Sensing Procedure

To evaluate the fluorescence sensing capability of the synthesized *Acer monspessulanum*-derived carbon quantum dots (CQDs) toward raloxifene, a standardized assay was developed. In each trial, 30 µg of CQDs was added to 3 mL of phosphate-buffered aqueous solution (pH 6.0), and the mixture was incubated under optimized conditions. Fluorescence emission spectra were recorded using an excitation

wavelength of 420 nm, with maximum emission intensity observed near 550 nm. The sensing response was determined by comparing the fluorescence intensity of the CQDs in the absence (F_0) and presence (F) of raloxifene. The quenching ratio (F_0/F) was calculated and plotted against varying concentrations of the target analyte to construct a calibration curve and assess linearity. This metric was used to determine the analytical performance parameters of the system. The limit of detection (LOD) was estimated based on a signal-to-noise (S/N) ratio of 3, in accordance with standard analytical guidelines, thereby establishing the minimum concentration of raloxifene that could be reliably detected using the developed fluorescence probe.

2.6. Machine Learning Analysis

To improve the accuracy and reliability of the fluorescence-based detection of raloxifene, multiple supervised machine learning models were implemented using Python (v3.13.2) in conjunction with the Scikit-learn library. Several regression algorithms—including support vector regression (SVR), random forest regression (RFR), artificial neural networks (ANN), k-nearest neighbors (KNN), gradient boosting regression (GBR), and decision tree regression (DTR)—were applied to the experimental dataset generated from fluorescence intensity measurements. Model performance was evaluated using standard statistical criteria such as the coefficient of determination (R^2), root mean square error (RMSE), and mean absolute error (MAE). The algorithm yielding the highest predictive power, indicated by a strong R^2 value and minimal error metrics, was identified as the most suitable model for accurate quantification of raloxifene concentrations. This approach highlights the synergy between nanomaterial-based sensing and data-driven prediction for enhanced analytical performance.

2.7. Preparation of sample

To investigate the real-world applicability of the developed CQDs-based fluorescence sensor, human plasma samples were utilized as a biological matrix. Fresh plasma specimens were collected from a certified clinical laboratory and stored at −20 °C until analysis. Prior to testing, the samples were thawed at room temperature and subjected to a deproteinization step to minimize matrix interference. In a typical procedure, 1.0 mL of plasma was transferred into a 10 mL centrifuge tube and mixed with 2.0 mL of 10% (w/v) trichloroacetic acid to precipitate plasma proteins. The mixture was vortexed for 2 minutes and sonicated at 25 °C for 10 minutes. Following this, centrifugation was carried out at 10,000 rpm for 15 minutes. The resulting clear supernatant was carefully separated, adjusted to pH 6.0 using dilute NaOH, and filtered through a 0.22 µm membrane to eliminate residual particulates. For recovery studies, selected plasma samples were spiked with known concentrations of raloxifene, processed identically, and analyzed using the optimized fluorescence sensing method.

2.8. Recovery Procedure

To assess the extraction efficiency and analytical applicability of the developed CQDs-based fluorescence sensor, recovery studies were performed using human plasma samples. Known concentrations of raloxifene were spiked into plasma at three different levels (low, medium, and high)

covering the linear dynamic range of the sensor. Each spiked sample underwent the same pretreatment protocol described in Section 2.7, including protein precipitation, centrifugation, neutralization, and filtration. Fluorescence measurements were then conducted under optimized conditions. All recovery experiments were carried out in triplicate to ensure reproducibility.

Results and discussion

3.1. Morphological and Elemental Characterization of CQDs

The morphological and compositional features of the synthesized carbon quantum dots (CQDs) were extensively evaluated through field emission scanning electron microscopy (FE-SEM), elemental mapping, and energy-dispersive X-ray spectroscopy (EDX). The SEM image (**Fig. 1(A)**) reveals that the particles possess a nearly spherical shape with smooth surfaces and uniform distribution at the nanoscale, indicating successful carbonization and the absence of significant aggregation. Elemental mapping results (**Fig.1 (B)**) confirmed the even distribution of primary and trace elements, suggesting good homogeneity across the CQDs surface. As demonstrated in the EDX spectrum (**Fig.1 (C)**), carbon and oxygen were the dominant constituents, with **carbon at 34.55 wt%** and **oxygen at 32.22 wt%**, confirming the organic and carbon-rich nature of the biosynthesized nanostructures. These two elements together accounted for over 66% of the total elemental composition, consistent with the expectations for carbon-based nanomaterials. Notably, several trace elements were also detected, including potassium (19.15 wt%), chlorine (5.52 wt%), calcium (4.16 wt%), magnesium (1.65 wt%), sodium (1.14 wt%), sulfur (0.93 wt%), and silicon (0.69 wt%). These residual elements likely originate from the intrinsic phytochemical composition of *Acer monspessulanum*, the natural precursor used in the green synthesis. The presence of such heteroatoms and mineral traces can play a significant role in modifying the surface functionality, enhancing hydrophilicity, and facilitating electron transfer—important factors for fluorescence sensing performance. The atomic percentages also reflect a high carbon (49.50%) and oxygen (34.66%) content, underscoring the abundance of C=O, C–O, and other oxygen-containing functional groups, which are vital for interaction with target molecules and enhancing quantum yield. Overall, these results validate the successful green synthesis of CQDs and confirm their compositional suitability for optical sensing applications.

To further investigate the surface chemical uniformity and bonding characteristics of the biosynthesized CQDs, EDX line scan analysis and FT-IR spectroscopy were performed. The EDX line profile (**Fig. 2(A)**) illustrates the spatial distribution of major and minor elements across a 30 µm line on the CQD surface. The most intense and consistent signals correspond to **carbon (C)**, **oxygen (O)**, and **potassium (K)**, reaffirming their dominance in the CQD matrix. Elements such as **chlorine (Cl)**, **calcium (Ca)**, and **magnesium (Mg)** displayed relatively lower but evenly distributed intensities, suggesting their presence as surface-bound residues likely inherited from the plant-based precursor material (*Acer monspessulanum*). The relatively stable signal profiles across the scanned region confirm the homogeneous distribution of elements within the synthesized nanomaterial. Complementary FT-IR analysis (**Fig. 2(B)**) was conducted to elucidate the surface functional groups present in the CQDs. The

broad absorption band centered at **3281 cm^{-1}** is attributed to **O–H and/or N–H stretching vibrations**, indicative of hydroxyl and amino functional groups commonly observed in carbon-based nanostructures. A prominent peak at **1637 cm^{-1}** corresponds to **C=O stretching** vibrations, confirming the presence of carbonyl functionalities. Additionally, the peak at **625 cm^{-1}** can be assigned to **C–H bending** or possible **metal–oxygen (M–O)** vibrations. These findings collectively demonstrate that the CQDs possess abundant surface functional groups capable of interacting with target analytes, thereby enhancing their fluorescence sensitivity and solubility in aqueous media.

The photoluminescence behavior of the synthesized carbon quantum dots (CQDs) was systematically investigated across a broad excitation wavelength range (280–380 nm) to determine their optimal optical performance. As illustrated in **Fig. 3**, the emission intensity of the CQDs was highly dependent on the excitation wavelength. Among the tested wavelengths, excitation at **360 nm** produced the most intense and well-defined emission peak centered around **453 nm**, indicating the most efficient excitation-emission pair for the as-prepared nanomaterial. This excitation-dependent emission behavior is characteristic of CQDs and is typically attributed to a combination of quantum confinement effects, surface state emissions, and diverse emissive traps originating from various surface functional groups. The strong and stable blue fluorescence under 360 nm excitation suggests excellent potential for the CQDs in sensitive fluorescence-based sensing applications.

Fig. 1

Fig. 2

Fig. 3

3.2. Statistical Optimization of Sensor Response via Response Surface Methodology

To achieve optimal fluorescence quenching efficiency F_0/F) in the detection of metronidazole using the synthesized carbon quantum dots (CQDs), a Response Surface Methodology (RSM) approach based on Central Composite Design (CCD) was employed. This design enabled the systematic assessment of three key variables—**pH (A)**, **temperature (B)**, and **reaction time (C)**—through 20 experimental runs. The experimental conditions and corresponding fluorescence responses are summarized in **Table 2**, where the observed values ranged from **1.5 to 1.82**, confirming the substantial influence of these parameters on the sensor performance. Among the tested statistical models (linear, interaction, and quadratic), the **quadratic model** showed the best performance in fitting the experimental data. As shown in **Table 3**, the model yielded a high **R^2 value of 0.9556**, along with an **adjusted R^2 of 0.9556** and **predicted R^2 of 0.8779**. The minor difference (<0.2) between the adjusted and predicted values reflects the model's reliability and low risk of overfitting. Furthermore, the **Adequate Precision ratio** of **16.20** (much higher than the desired threshold of 4) indicates an excellent signal-to-noise ratio, affirming the model's robustness for exploring the design space. The final regression equation in terms of coded variables is:

$$F_0/F=1.0882+0.0902A+0.0061B+0.0708C+0.055AC+0.0281A_2-0.0067B_2-0.0009C_2 \quad \textbf{Eq. 2}$$

In this equation, positive coefficients denote synergistic effects, particularly for **pH (A)** and **reaction time (C)**, both individually and through their interaction (AC). Meanwhile, the negative quadratic terms for **temperature (B^2)** and **reaction time (C^2)** suggest inhibitory effects at extreme values. These findings underscore the critical role of parameter tuning in maximizing sensor performance. Collectively, the results validate the **quadratic model** as a predictive and effective tool for optimizing operational parameters, providing a solid basis for practical application of the CQDs-based fluorescence sensor.

Table 2

Table 3

3.3. ANOVA

Based on the ANOVA results for the quadratic model (**Table 4**), the overall model was statistically significant, with an F-value of 44.07 and a corresponding p-value < 0.0001, indicating that the variation explained by the model is highly unlikely to be due to random noise. Among the individual factors, pH (A) and reaction time (C) were identified as highly significant variables, with p-values < 0.0001. In addition, the interaction between pH and time (AC) and the quadratic term of time (C^2) also exhibited significant effects on the response, confirming their substantial contributions. In contrast, temperature (B) and its quadratic term (B^2), as well as the interactions AB and BC, were not statistically significant, suggesting minimal impact within the studied range. Furthermore, the lack of fit was not significant (F = 1.05, p = 0.4935), supporting the adequacy of the model in capturing the experimental data. The residual and pure errors were small, further reinforcing the robustness and predictive capability of the quadratic model for optimizing the sensor's performance.

Table 4

3.4. 3D Response Surface Plots

Three-dimensional response surface plots were generated to investigate the individual and interactive effects of pH (A), temperature (C), and reaction time (B) on the fluorescence quenching response (F_0/F), based on the fitted quadratic model (**Fig. 4A–C**). In **Fig.4A**, the interaction between pH and temperature is illustrated. The response surface demonstrates moderate curvature, suggesting a noticeable but not dominant interaction. As pH increases, the fluorescence response initially rises and then plateaus, while changes in temperature show a slight modulation of this trend. The nearly linear and parallel contour lines imply that pH plays a more substantial role than temperature, which may be due to the thermosensitivity of the probe being limited within the experimental range. In **Fig.4B**, the interaction between pH and reaction time exhibits a more pronounced curvature, along with elliptical contour lines. The fluorescence response increases with both pH and time, reaching a maximum before declining, indicating a significant synergistic interaction. This pattern reflects a nonlinear dependency, which likely arises from optimal surface-state interactions or aggregation dynamics at certain pH-time combinations that enhance quenching efficiency. **Fig.4C** explores the interaction between temperature and reaction

time. Here, the response surface appears relatively flat, and the contour lines are almost parallel, indicating a weak interaction between these variables. While a slight increase in fluorescence quenching is observed with increasing reaction time, temperature has minimal influence over the studied range. This suggests that the quenching process is more time-dependent, while temperature does not substantially affect the molecular interaction mechanisms under these conditions. Overall, the plots confirm that pH and reaction time are the most influential factors, while temperature plays a secondary role. The presence of well-defined optima in the response surfaces further underscores the utility of response surface methodology (RSM) in optimizing experimental conditions for maximal sensor performance.

Fig.4

3.5. Statistical Evaluation of the Quadratic Model for Fluorescence Quenching Response

The statistical analysis of the quadratic model developed for predicting the fluorescence quenching response (F_0/F) is summarized in Table 5, confirming its strong performance and reliability. The coefficient of determination (R^2) was 0.9778, indicating that 97.78% of the variability in the response was explained by the model. The adjusted R^2 of 0.9556 and the predicted R^2 of 0.8779 were in reasonable agreement (difference < 0.2), further supporting the model's robustness and predictive capability. The standard deviation (SD) of 0.0227 and a low coefficient of variation (C.V.) of 1.41% demonstrate minimal experimental error and high precision. Moreover, the adequate precision value of 21.48, which is well above the threshold of 4, highlights a strong signal-to-noise ratio and confirms the suitability of the model for navigating the design space. Collectively, these statistical parameters validate the accuracy, precision, and applicability of the quadratic model in optimizing the fluorescence sensing system.

Table 5

3.6. Model Diagnostics and Assumptions Verification

To assess the statistical integrity and adequacy of the developed quadratic model, a series of diagnostic plots were examined (**Fig.5 A–D**). These plots facilitate the evaluation of critical regression assumptions, including normality, homoscedasticity, and independence of residuals. In **Fig. 5A** (Residuals vs. Predicted Values), the residuals are evenly dispersed around the horizontal axis with no discernible pattern, suggesting homoscedasticity and consistent variance across predicted values, which is a fundamental requirement in regression analysis. **Fig.5B** (Normal Probability Plot of Residuals) illustrates that the residuals closely follow a straight line, indicating an approximate normal distribution and minimal skewness or influential outliers, thereby supporting the model's validity. In **Fig.5 C** (Predicted vs. Actual Values), the majority of points cluster near the diagonal line, demonstrating strong concordance between predicted and experimental values. However, slight deviations at extreme values suggest potential minor over- or under-prediction in those regions. **Fig. 5D** (Residuals vs. Run Order) reveals no systematic trends, confirming the independence of residuals and the absence of temporal biases in the experimental process. Collectively, these diagnostic plots validate the model's adherence to essential

regression assumptions, affirming its reliability and robustness for predictive and optimization purposes in the studied application.

Fig.5

3.7. Machine Learning Model Evaluation for Metronidazole Prediction

The 3D performance comparison plot (**Fig.6 A**) illustrates the trade-off between R^2, RMSE, and MAE across the three models. The Random Forest model stands out with the lowest RMSE (~0.03) and MAE (~0.02), indicating high precision and minimal average error in predicting the fluorescence quenching response. Its positioning in the optimal region of the plot reflects its superior ability to model the nonlinear relationships in the data. In contrast, Linear Regression and SVR exhibit higher RMSE (~0.08 and ~0.10, respectively) and MAE (~0.06 and ~0.07, respectively), suggesting larger deviations between predicted and actual values. This clustering in a less favorable region of the plot underscores their struggle to capture the dataset's complexity, likely due to their reliance on linear or kernel-based assumptions that do not generalize well. The Actual vs. Predicted plot (**Fig. 6B**) reinforces this, with Random Forest predictions (green points) closely aligning with the diagonal line, while Linear Regression (red) and SVR (blue) show greater scatter, consistent with their higher error metrics.

Fig.6

3.8. Method Selectivity

To evaluate the selectivity of the developed sensing platform, a series of potentially interfering compounds were tested under identical conditions, including dopamine, phenobarbital, isoniazid, nevirapine, efavirenz, tenofovir, phenol, thiourea, glucose, catechol, L-cysteine, and sumatriptan. The normalized fluorescence responses of these analytes were consistently close to unity, indicating negligible interference with the sensing system. In sharp contrast, raloxifene induced a significant enhancement in fluorescence intensity, reaching a normalized value of 1.23. This pronounced difference highlights the exceptional selectivity of the sensor toward raloxifene, while demonstrating minimal cross-reactivity with other structurally or functionally related compounds. Such specificity underscores the system’s promise for reliable raloxifene detection in complex matrices.

Fig.7

3.9. Calibration and Detection of raloxifene

In this study, carbon quantum dots (CQDs) were green-synthesized through a sustainable hydrothermal approach using Acer monspessulanum leaf extract as a renewable carbon source. The resulting CQDs exhibited a pronounced fluorescence emission that was significantly enhanced upon interaction with raloxifene (RLX), laying the groundwork for their application as an eco-friendly fluorescence sensor. Under optimized experimental conditions, the fluorescence intensity of the CQDs increased progressively with increasing RLX concentrations, facilitating sensitive detection. To evaluate the sensor’s analytical

performance, RLX concentrations ranging from 10.0 to 750.0 μM were introduced into the sensing system, and the fluorescence intensity ratio (F_0/F) was plotted as a function of RLX concentration. As shown in **Fig. 8A**, the sensor demonstrated a distinct linear response across this range, supported by a high correlation coefficient (R^2), indicating excellent linearity and precision. The limit of detection (LOD) and limit of quantification (LOQ), calculated based on the standard deviation of the blank and the slope of the calibration curve, were determined to be 1.27 μM and 3.82 μM, respectively (**Fig. 8B**), highlighting the sensor's high sensitivity. This fluorescence enhancement is likely attributed to the interaction between raloxifene and the CQDs' surface functional groups, potentially altering the electronic environment and promoting radiative recombination. The robust linearity and low detection limits affirm the CQDs-based sensor's capability for accurate and reliable quantification of raloxifene in aqueous samples.

Fig.8

3.10. Interference Study for raloxifene Detection

To evaluate potential interferences in the determination of raloxifene, common plasma constituents were introduced into the test system. The fluorescence intensity of 250 μM raloxifene was measured in the absence and presence of 500 μM of each possible interfering compound, including Calcium (Ca^{2+}), Potassium (K^+), Sodium (Na^+), Glucose, Albumin, Ascorbic acid (Vitamin C), Riboflavin (Vitamin B2), Triglycerides, and Lactic acid. The obtained results showed negligible changes in the fluorescence response, confirming that these substances exert no significant effect on raloxifene detection. These findings highlight the excellent selectivity of the CQDs-based sensor and demonstrate its suitability for reliable quantification of raloxifene in complex plasma matrices (**Fig.9**).

Fig.9

3.11. Applications in Plasma Samples

To evaluate the practical applicability of the developed CQDs-based fluorescent sensor, human plasma was employed as a representative real sample due to its clinical relevance. Plasma samples were pretreated by protein precipitation followed by dilution with phosphate buffer (pH 7.4) to reduce matrix effects and simulate physiological conditions. Under optimized conditions, the sensor's performance was assessed by spiking known concentrations of raloxifene (15, 200,500 and 700 μM) into the treated plasma matrices. Fluorescence signals were recorded, and raloxifene concentrations were quantified using the established calibration curve. As summarized in **Table 6**, the calculated recoveries were 10.1%, 100.51.2%, 100.83% and 100.13% for the respective spiked levels. Moreover, the method demonstrated strong precision, with relative standard deviation (RSD%) values of 3.0%, 2.34%,1.25% and 0.93%. These results confirm the sensor's high reliability for raloxifene determination in complex plasma matrices and underline its potential for clinical and pharmacokinetic applications.

Recovery Study in Plasma Samples

The reliability and accuracy of the developed fluorescence sensor were further validated through recovery experiments. The obtained recovery values ranged from 94.2% to 102.5%, reflecting high extraction efficiency and negligible matrix interference. Additionally, the RSD values for triplicate measurements remained below 4.0%, confirming the excellent repeatability of the method. Collectively, these findings highlight the robustness of the proposed CQDs-based sensor and its suitability for routine pharmacological monitoring of raloxifene in plasma samples. **Table 7** summarizes the analytical performance of several fluorescence-based methods reported for raloxifene detection. Different strategies, including micelle and metal complexation, gold–chitosan hydrogel, Zn-based metal–organic frameworks, and g-C_3N_4-Co-Fe nanocomposites, have been explored, each offering distinct advantages in terms of sensitivity and linear range. Among these, the Zn-MOF system demonstrated the lowest LOD (0.485 nM), while g-C_3N_4-Co-Fe and micelle-based methods provided broader but relatively less sensitive ranges. In comparison, the CQDs synthesized from Acer monspessulanum in the present work achieved a wide linear range (10.0–750.0 μM) with an acceptable LOD of 1.27 μM, demonstrating a balance between sensitivity, eco-friendliness, and cost-effectiveness. These results highlight the potential of green-synthesized CQDs as a competitive alternative for raloxifene detection, particularly in applications where sustainability and practicality are prioritized alongside analytical performance [7,8,13,14].

Table 6

Table 7

Conclusions

This research presents the development of an innovative, environmentally sustainable, and highly sensitive fluorescence-based sensor utilizing carbon quantum dots (CQDs) synthesized from Acer monspessulanum via a green hydrothermal process. Comprehensive characterization through advanced techniques such as fluorescence spectroscopy, FTIR, SEM, EDX, and elemental mapping validated the CQDs' unique structural and luminescent properties. The sensor effectively harnessed a fluorescence quenching mechanism to detect raloxifene (RLX), achieving an optimized linear detection range (10.0 to 750.0 μM) and a notably low limit of detection (1.27 μM) alongside a limit of quantification (3.82 μM), as refined through Response Surface Methodology (RSM) with Design-Expert software. The sensor's precision was further evidenced by its commendable repeatability and reproducibility metrics. Incorporation of machine learning techniques provided enhanced predictive capabilities, offering valuable insights into the interplay of experimental variables and bolstering the sensor's analytical robustness. Selectivity assessments revealed minimal interference from structurally diverse compounds, affirming the sensor's specificity for raloxifene. Validation in spiked real samples demonstrated consistent performance with negligible matrix effects and robust recovery rates, underscoring its practical utility. Collectively, this CQDs-based sensor emerges as a cost-effective, eco-conscious solution for the precise monitoring of pharmaceutical residues, with significant potential for application in environmental and biological matrices, contributing to advanced pharmaceutical surveillance and safety protocols.

Declarations

Acknowledgements

The authors would like to thank Islamic Azad University of Sanandaj for providing laboratory facilities and support.

Authors' contributions

Neda Alaei and Nahid Haghnazari: Performed the experimental work, collected data, and contributed to the initial draft of the manuscript.

Bahareh Rahimian Zarif: Conceived and designed the study, supervised the project, analyzed the data, and revised the manuscript critically.

All authors read and approved the final manuscript.

Competing interests

The authors declare that they have no known competing financial interests or personal relationships that could have appeared to influence the work reported in this paper.

Data availability

All data generated or analyzed during this study are available from the corresponding author upon reasonable request.

Ethics declarations

All milk samples used in this study were commercially available and purchased from local dairy sources in Kermanshah. The samples were used solely for analytical purposes, and no human or animal subjects were directly involved. Therefore, ethical approval and informed consent were not required for this study.

Consent to participate / Consent for publication

Not applicable.

Funding

This research did not receive any specific grant from funding agencies in the public, commercial, or not-for-profit sectors.

References

1. Seidi, S.; Alavi, L.; Jabbari, A.; Shanehsaz, M. Three-Phase Carrier-Mediated Hollow Fiber Microextraction Based on Deep Eutectic Solvent Followed by HPLC--UV for Determination of Raloxifene and Ethinylestradiol in Pharmaceutical Wastewater Treatment Plants. *Journal of the Iranian Chemical Society* **2019**, *16*, 1007–1018.
2. Yang, Z.; He, X.; Zhang, Y. The Determination of Raloxifene in Rat Tissue Using HPLC. *Biomedical Chromatography* **2007**, *21*, 229–233.
3. Patel, V.; Patel, C.; Patel, B.; Thakkar, H. Formulation and Evaluation of Raloxifene Hydrochloride Dry Emulsion Tablet Using Solid Carrier Adsorption Technique. *Therapeutic Delivery* **2021**, *12*, 539–552.
4. Mahmood, S.; Mandal, U.K.; Chatterjee, B. Transdermal Delivery of Raloxifene HCl via Ethosomal System: Formulation, Advanced Characterizations and Pharmacokinetic Evaluation. *International journal of pharmaceutics* **2018**, *542*, 36–46.
5. Ghalkhani, M.; Shahrokhian, S.; Navabi, M. Development of an Electrochemical Sensor Based on (rGO-CNT) Nanocomposite for Raloxifene Analysis. *Materials Chemistry and Physics* **2021**, *263*, 124131.
6. Bagheri, A.; Hosseini, H. Electrochemistry of Raloxifene on Glassy Carbon Electrode and Its Determination in Pharmaceutical Formulations and Human Plasma. *Bioelectrochemistry* **2012**, *88*, 164–170.
7. Wu, Y.; Jin, X.; Afshar, E.A.; Taher, M.A.; Xia, C.; Joo, S.-W.; Mashifana, T.; Vasseghian, Y. Simple Turn-off Fluorescence Sensor for Determination of Raloxifene Using Gold Nanoparticles Stabilized by Chitosan Hydrogel. *Chemosphere* **2022**, *305*, 135392.
8. Ibrahim, F.; El-Enany, N.; El-Shaheny, R.; Mikhail, I. Study of Micelle and Metal Complexation-Mediated Fluorescence Enhancements of Raloxifene Hydrochloride. Application to Pharmaceutical Analysis. *Journal of Molecular Liquids* **2018**, *252*, 408–415.
9. Kneipp, J.; Kneipp, H.; Wittig, B.; Kneipp, K. Novel Optical Nanosensors for Probing and Imaging Live Cells. *Nanomedicine: Nanotechnology, Biology and Medicine* **2010**, *6*, 214–226.
10. Hou, J.; Li, H.; Wang, L.; Zhang, P.; Zhou, T.; Ding, H.; Ding, L. Rapid Microwave-Assisted Synthesis of Molecularly Imprinted Polymers on Carbon Quantum Dots for Fluorescent Sensing of Tetracycline in Milk. *Talanta* **2016**, *146*, 34–40.
11. Liu, G.; Chen, Z.; Jiang, X.; Feng, D.-Q.; Zhao, J.; Fan, D.; Wang, W. In-Situ Hydrothermal Synthesis of Molecularly Imprinted Polymers Coated Carbon Dots for Fluorescent Detection of Bisphenol A. *Sensors and Actuators B: Chemical* **2016**, *228*, 302–307.
12. Jain, P.K.; Huang, X.; El-Sayed, I.H.; El-Sayed, M.A. Noble Metals on the Nanoscale: Optical and Photothermal Properties and Some Applications in Imaging, Sensing, Biology, and Medicine. *Accounts of chemical research* **2008**, *41*, 1578–1586.
13. Rani, S.; Bandyopadhyay-Ghosh, S.; Ghosh, S.B.; Liu, G. In-Situ Detection of Bone Cancer Using Nanomaterial Based Surface Modulated Biosensors. In Proceedings of the AIP Conference Proceedings; 2023; Vol. 2752.

14. Afarani, N.H.; Keshavarzi, F.; Shahanipour, K.; Zarei, S.A. Detection of Raloxifene Using a Modified Carbon Nitride Graphite with Cobalt and Iron as a Turn-off Fluorescence Sensor. *Water, Air, & Soil Pollution* **2025**, *236*, 455.

Tables

Table 1: Experimental parameters and levels in the 20 CCD for the optimization of pH, Temp, and Time

Factor	Name	Level	Low Level	High Level	Std. Dev.	Coding
A	pH	6.00	3.00	9.00	0.0000	Actual
B	temperature	45.00	30.00	60.00	0.0000	Actual
C	time	9.00	3.00	15.00	0.0000	Actual

Table 2: Experiment runs and responses for optimizing parameters evaluation

	Factor 1	Factor 2	Factor 3	Response 1
Run	A: pH	B: Temp	C: Time	F_0/F
1	9	60	15	1.82
2	3	60	3	1.5
3	6	45	9	1.55
4	6	70	9	1.6
5	6	20	9	1.55
6	10	45	9	1.72
7	6	45	19	1.82
8	3	30	3	1.5
9	6	45	9	1.6
10	9	60	3	1.55
11	6	45	1	1.53
12	6	45	9	1.6
13	3	30	15	1.55
14	9	30	15	1.82
15	1	45	9	1.5
16	6	45	9	1.6
17	9	30	3	1.55
18	6	45	9	1.6
19	3	60	15	1.55
20	9	60	15	1.82

Table 3: Model summary statistic.

Source	Sequential p-value	Lack of Fit p-value	Adjusted R^2	Predicted R^2	
Linear	< 0.0001	0.0431	0.7840	0.6681	
2FI	0.0050	0.1635	0.9038	0.8684	
Quadratic	**0.0185**	**0.4935**	**0.9556**	**0.8779**	**Suggested**
Cubic	0.4935		0.9569		Aliased

Table 4: ANOVA for response surface quadratic model for F_0/F

Source	Sum of Squares	df	Mean Square	F-value	p-value	
Model	0.2042	9	0.0227	44.07	< 0.0001	significant
A-pH	0.0741	1	0.0741	143.98	< 0.0001	
B-temperature	0.0005	1	0.0005	0.9948	0.3446	
C-time	0.0846	1	0.0846	164.22	< 0.0001	
AB	0.0000	1	0.0000	0.0000	1.0000	
AC	0.0242	1	0.0242	46.99	< 0.0001	
BC	0.0000	1	0.0000	0.0000	1.0000	
A^2	0.0005	1	0.0005	1.06	0.3293	
B^2	0.0015	1	0.0015	2.95	0.1197	
C^2	0.0061	1	0.0061	11.82	0.0074	
Residual	0.0046	9	0.0005			
Lack of Fit	0.0026	5	0.0005	1.05	0.4935	not significant
Pure Error	0.0020	4	0.0005			
Cor Total	0.2089	18				

Table 5: Standard deviation and R^2 of the response.

Std. Dev.	0.0227	**R^2**	0.9778
Mean	1.61	**Adjusted R^2**	0.9556
C.V. %	1.41	**Predicted R^2**	0.8779
		Adeq Precision	21.4828

Table 6: Determination of Raloxifene concentration in real samples. By fluorescence method (n = 5)

sample	Spiked value Raloxifene (μM)	Found value by the sensor Raloxifene (μM)	RSD%	Recovery (%)
1	15	15.16 ±0.456	3.0	101.1
2	200	201.02±4.89	2.34	100.51
3	500	502.38±6.26	1.25	100.83
4	700	700.94±6.43	0.93	100.13

Relative standard error: RSD

Table 7. Comparison of different fluorescence methods for raloxifene detection.

Methods used	Linear range	LOD	Ref.
micelle and metal complexation	0.01 and 0.02 μg/mL	0.02 μg/mL	[12]
Gold-chitosan hydrogel	5×10^{-7} to 5×10^{-5} M	34×10^{-8} M	[13]
Zn metal-organic framework	0.7 to 350 ng/mL	0.485 nM	[34]
g-C_3N_4-Co-Fe	10.0-500.0	5.0μM	[25]
CQDs by *Acer monspessulanum*	10.0-750.0	1.27 μM	Current work

Figures

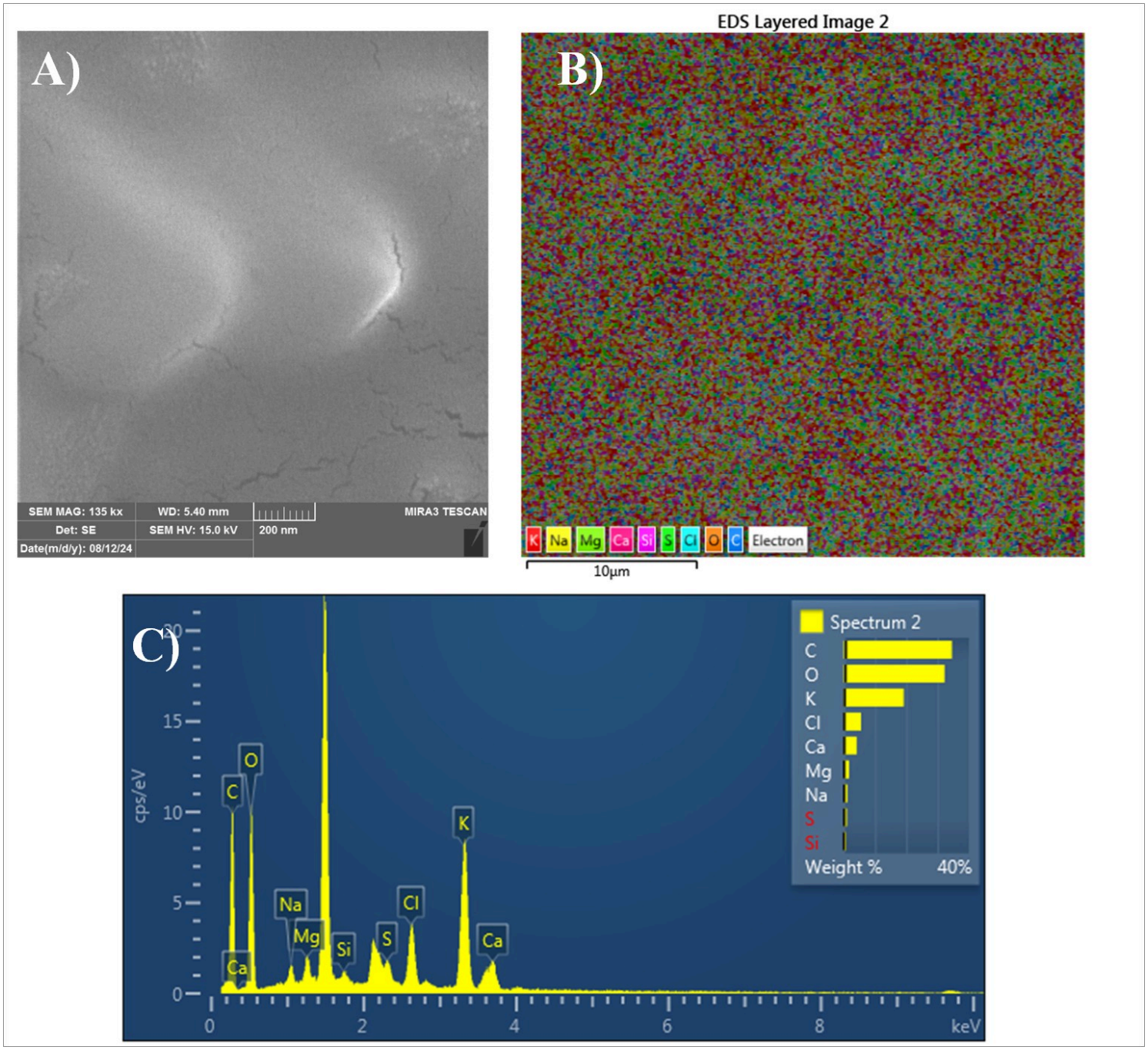

Figure 1

A) SEM images, B) mapping imaging, **C**) EDS of CQDs

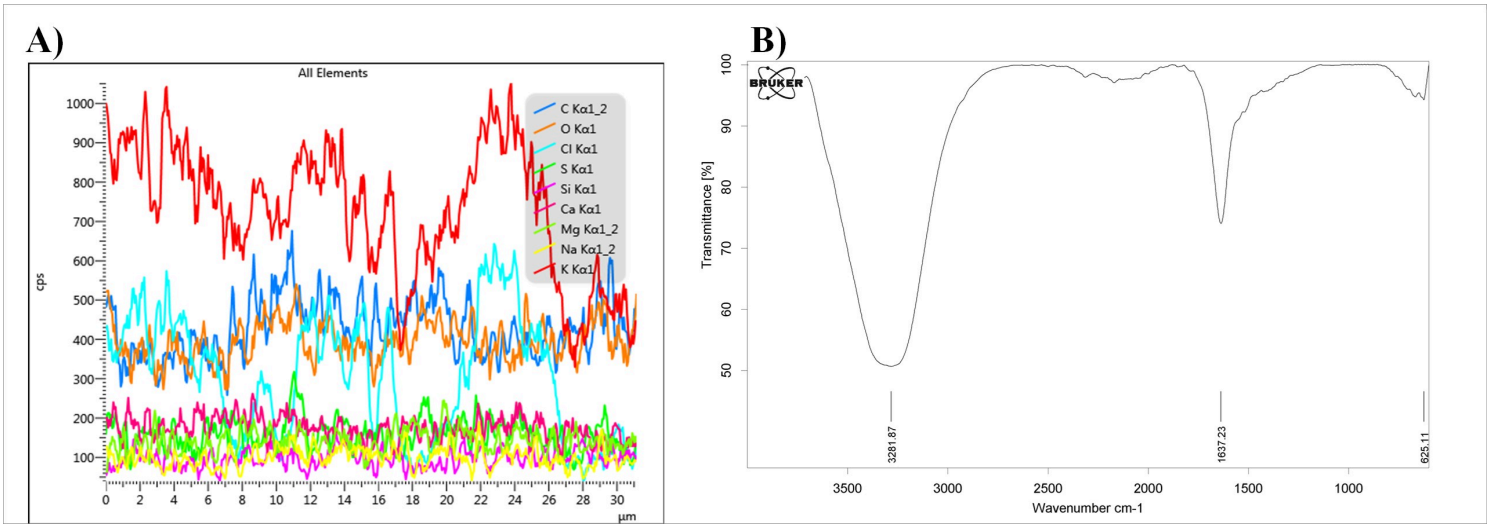

Figure 2

A) line scanning of R-CQDs, **B**) FTIR spectra of CQDs

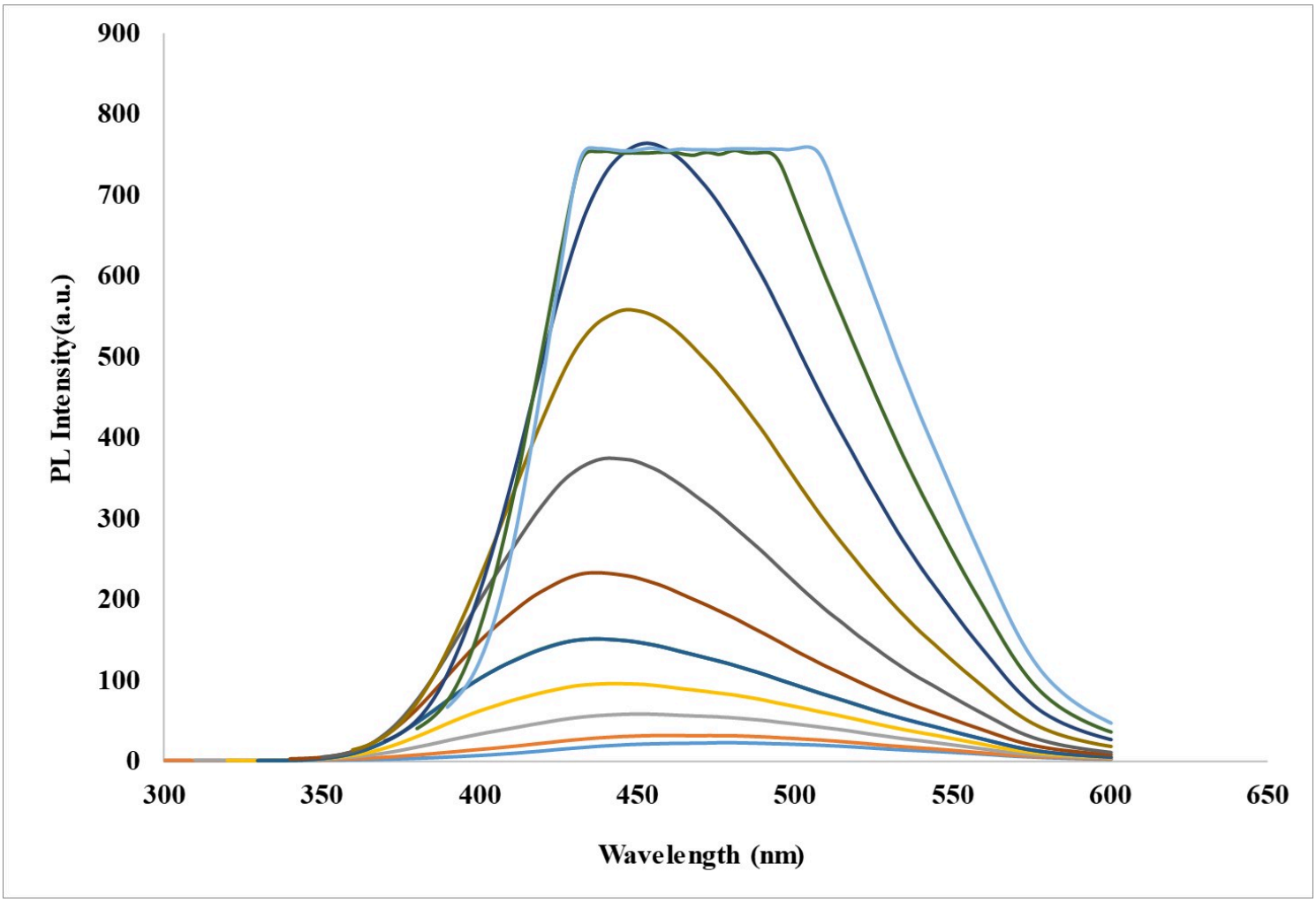

Figure 3

Fluorescence spectrum of CQDs in excitation with different wavelengths from 280 nm to 380 nm

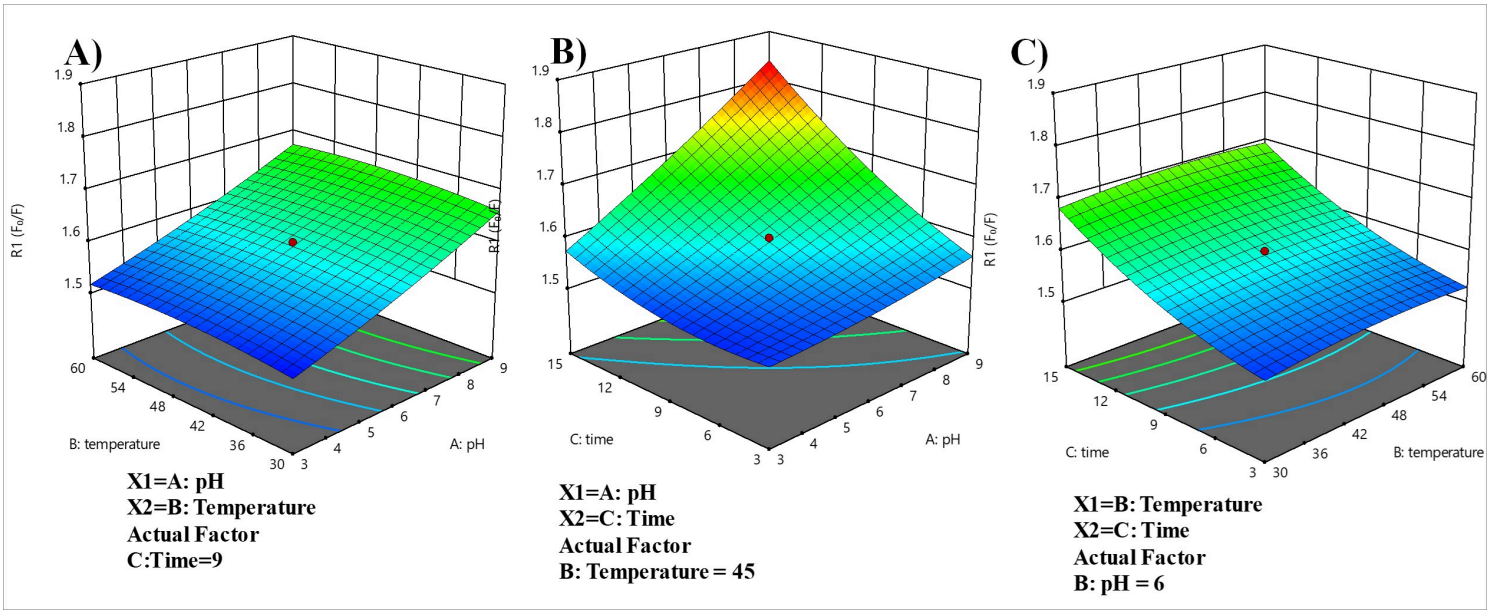

Figure 4

Response surface plots illustrating the effects of (A) pH–temperature, (B) pH–time, and (C) temperature–time on the fluorescence quenching response (F_0/F). pH and time emerged as the dominant factors, while temperature showed a minor influence within the studied range.

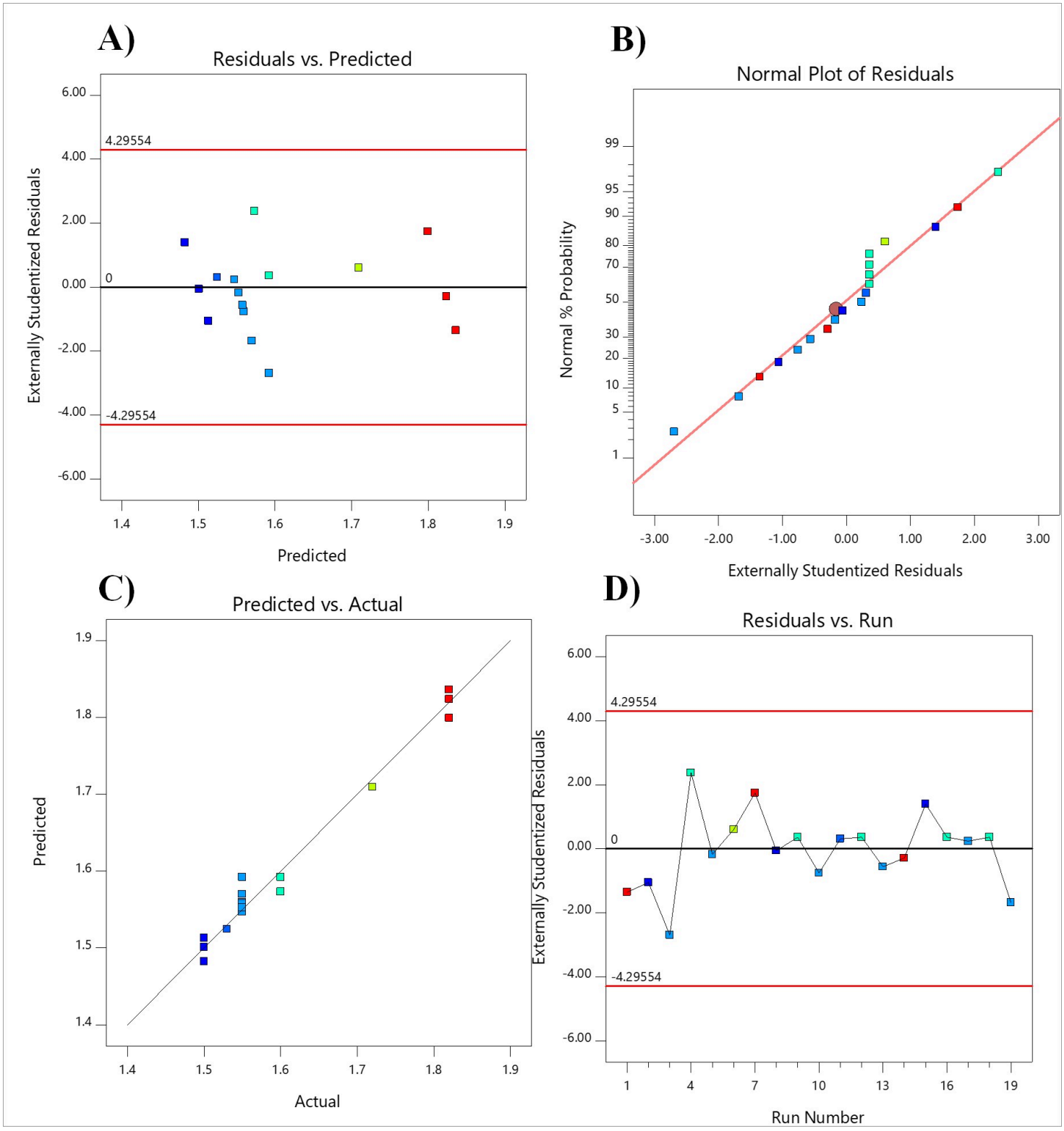

Figure 5

Diagnostic plots of the quadratic model: (A) residuals vs. predicted values, (B) normal probability plot of residuals, (C) predicted vs. actual values, and (D) residuals vs. run order. The plots confirm normality, homoscedasticity, independence of residuals, and strong agreement between predicted and experimental values, validating the model's adequacy and robustness.

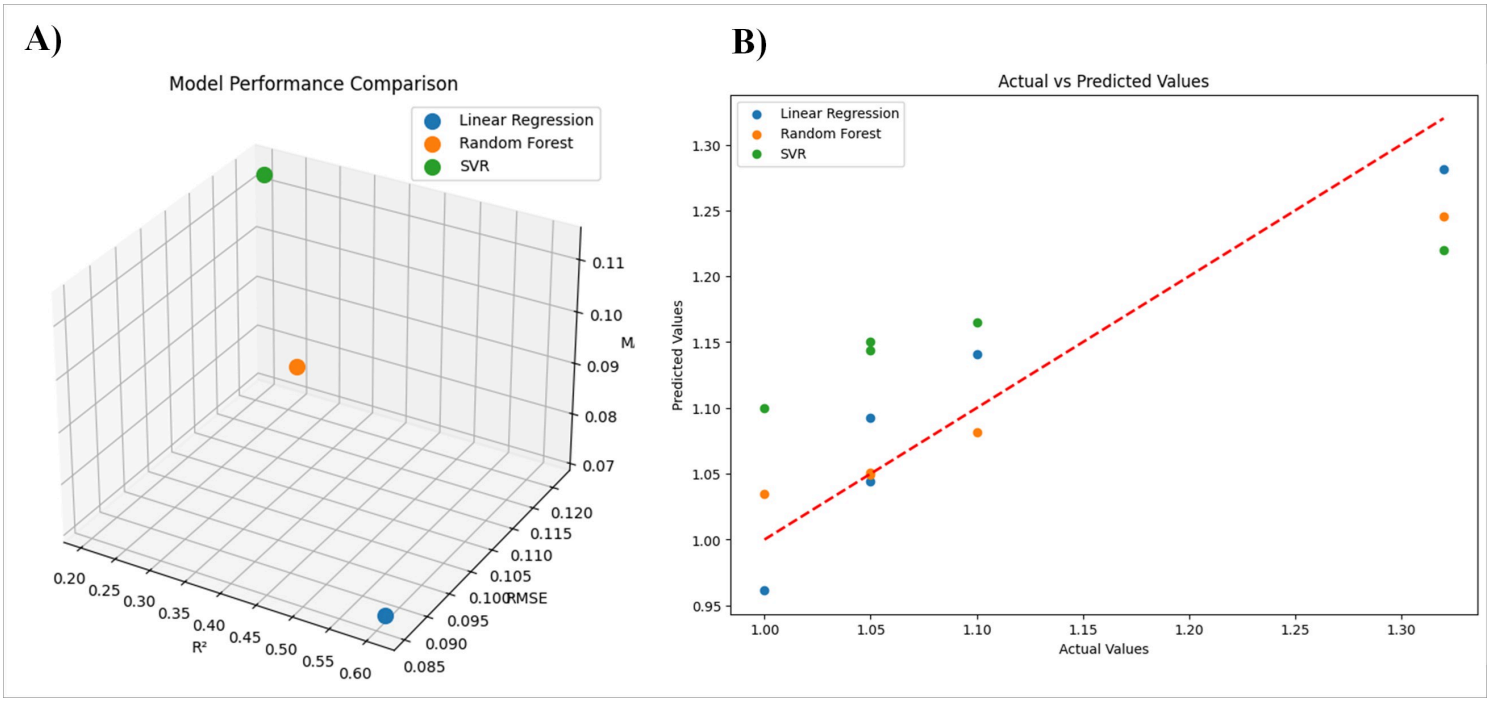

Figure 6

Model performance comparison: (A) 3D plot of R^2, RMSE, and MAE for Random Forest, Linear Regression, and SVR, showing Random Forest with the lowest errors and superior predictive ability; (B) actual vs. predicted values, where Random Forest aligns closely with the diagonal line, while Linear Regression and SVR exhibit larger deviations.

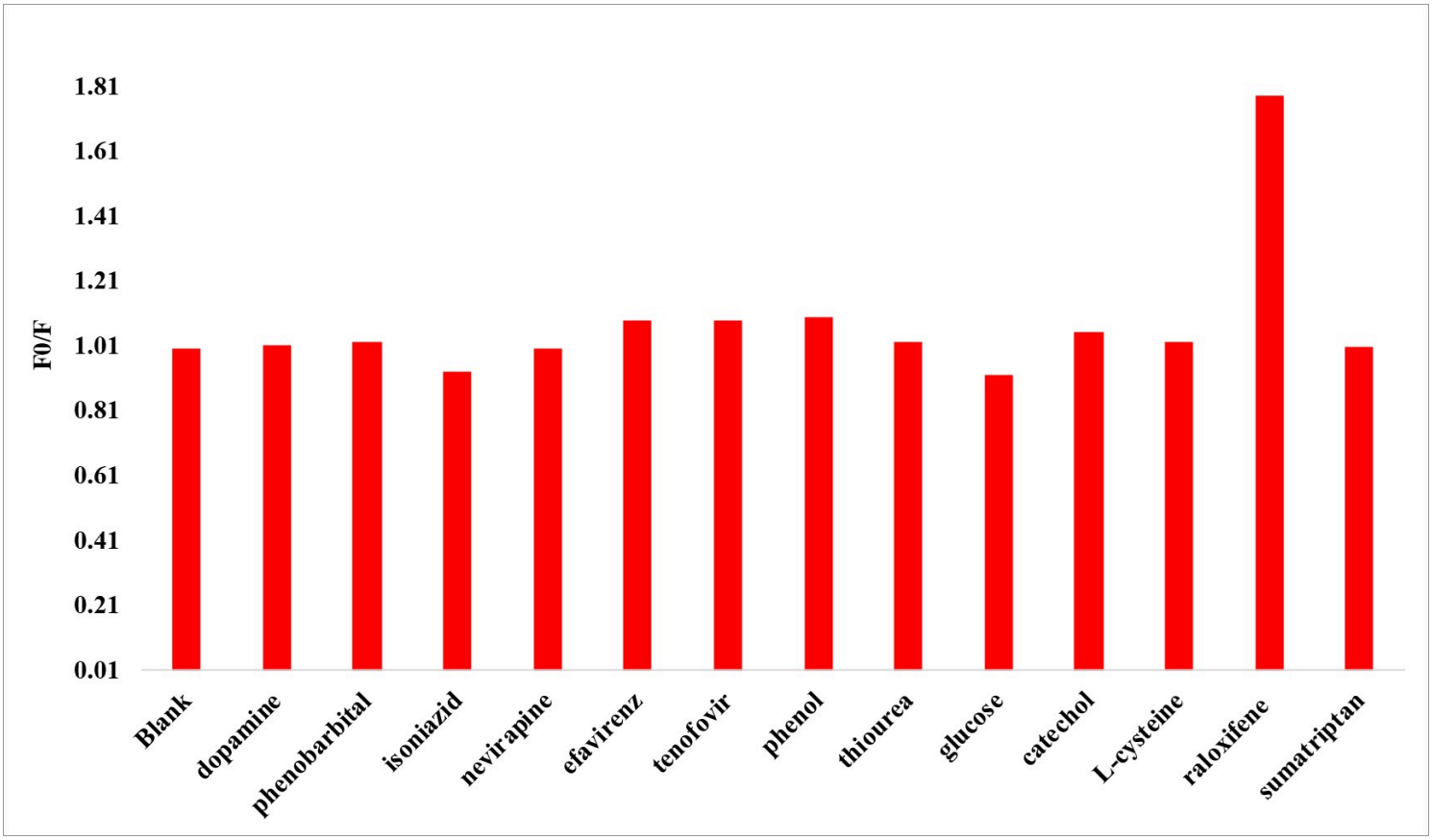

Figure 7

Selectivity study of the developed fluorescence sensor toward raloxifene against common potential interferents, showing a pronounced response exclusively for raloxifene while other analytes exhibited negligible effects.

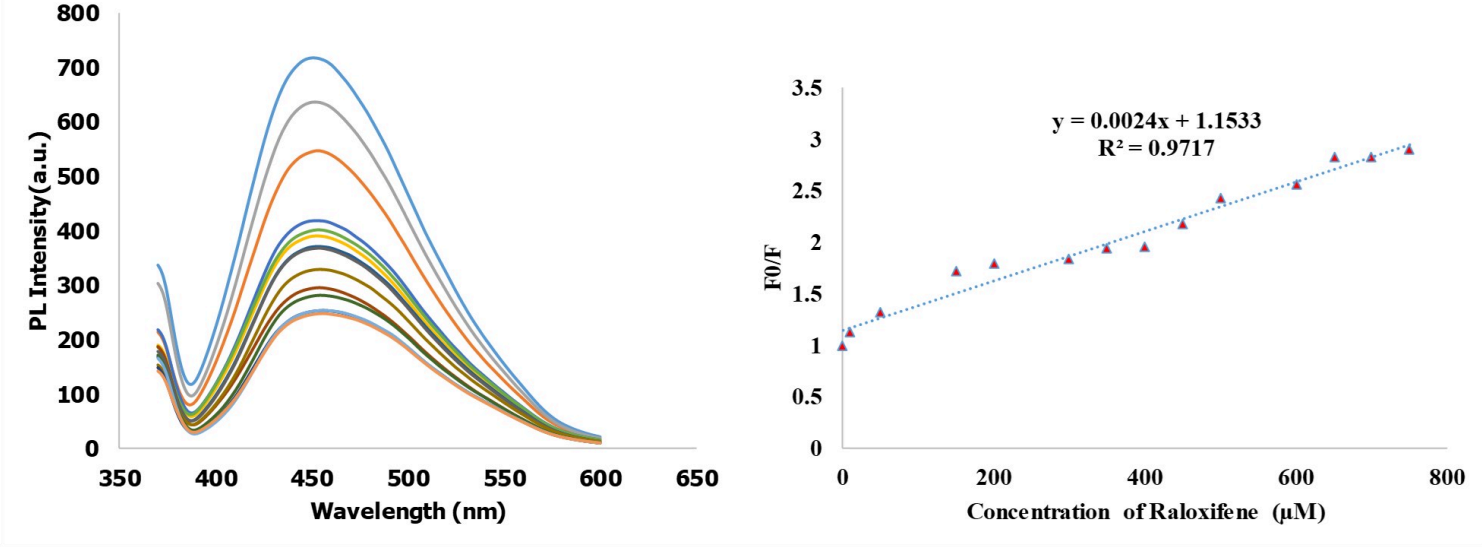

Figure 8

Calibration curve for raloxifene detection using CQDs-based fluorescence sensor. The sensor shows a linear response from 10.0 to 750.0 µM, with LOD of 1.27 µM and LOQ of 3.82 µM, demonstrating high sensitivity and precision.

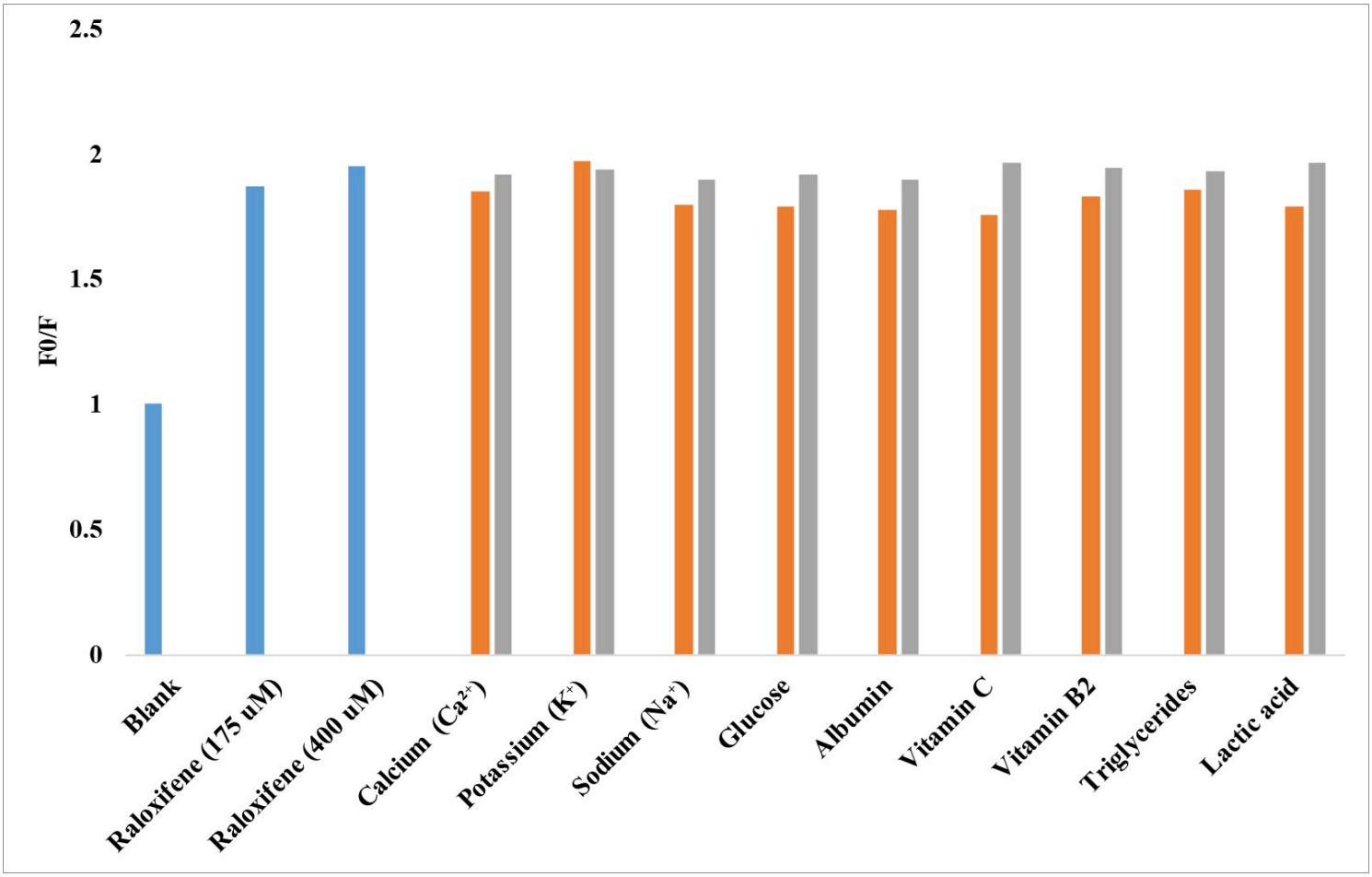

Figure 9

Interference study showing negligible effect of common plasma constituents on the fluorescence detection of 175 µM and 400 µM raloxifene, demonstrating high sensor selectivity.